Clinical Potential of UTE-MRI for Assessing COVID-19: Patient- and Lesion-Based Comparative Analysis

Shuyi Yang PhD, MD,[1†] Yunfei Zhang PhD,[2†] Jie Shen B.S.,[1] Yongming Dai PhD,[2]

Yun Ling MD,[3] Hongzhou Lu PhD, MD,[3] Rengyin Zhang B.S.,[1] Xueting Ding B.S.,[1]

Huali Qi B.S.,[1] Yuxin Shi PhD, MD,[1] Zhiyong Zhang PhD, MD,[1,4]* and Fei Shan PhD, MD[1]*

Background: Chest computed tomography (CT) has shown tremendous clinical potential for screening, diagnosis, and surveillance of COVID-19. However, safety concerns are warranted due to repeated exposure of X-rays over a short period of time. Recent advances in MRI suggested that ultrashort echo time MRI (UTE-MRI) was valuable for pulmonary applications.
Purpose: To evaluate the effectiveness of UTE-MRI for assessing COVID-19.
Study Type: Prospective.
Population: In all, 23 patients with COVID-19 and with an average interval of 2.81 days between hospital admission and image examination.
Field strength/Sequence: 3T; Respiratory-gated three-dimensional radial UTE pulse sequence.
Assessment: Image quality score. Patient- and lesion-based interobserver and intermethod agreement for identifying the representative image findings of COVID-19.
Statistical Tests: Wilcoxon-rank sum test, Kendall's coefficient of concordance (Kendall's W), intraclass coefficients (ICCs), and weighted kappa statistics.
Results: There was no significant difference between the image quality of CT and UTE-MRI (CT vs. UTE-MRI: 4.3 ± 0.4 vs. 4.0 ± 0.5, $P = 0.09$). Moreover, both patient- and lesion-based interobserver agreement of CT and UTE-MRI for evaluating the image signs of COVID-19 were determined as excellent (ICC: 0.939–1.000, $P < 0.05$; Kendall's W: 0.894–1.000, $P < 0.05$.). In addition, the intermethod agreement of two image modalities for assessing the representative findings of COVID-19 including affected lobes, total severity score, ground glass opacities (GGO), consolidation, GGO with consolidation, the number of crazy paving pattern, and linear opacities, as well as pseudocavity were all determined as substantial or excellent (kappa: 0.649–1.000, $P < 0.05$; ICC: 0.913–1.000, $P < 0.05$).
Data Conclusion: Pulmonary MRI with UTE is valuable for assessing the representative image findings of COVID-19 with a high concordance to CT.
Evidence Level: 2
Technical Efficacy Stage: 3

SINCE THE OUTBREAK in Wuhan, China, in December, 2019, COVID-19 has rapidly spread worldwide. As of May 3, there were more than 3.3 million confirmed cases and 238 000 deaths in 211 countries.[1] The United States, Spain, Italy, the United Kingdom, Germany, France, Russian, and Turkey all have more than 100 000 cumulative confirmed cases.[1] A worldwide consensus has been reached that this is an unprecedented human public health emergency. At present, real-time reverse transcription polymerase chain reaction (RT-PCR) is accepted as the standard diagnostic criterion for COVID-19.[2] Nevertheless, 1) it's difficult to address the challenges caused by the surge in diagnostic

demand with limited manufacturing capacity of RT-PCR kits, especially in less-developed countries. 2) False-negative RT-PCR results have been broadly reported.[3,4] Given the aforementioned challenges, chest computed tomography (CT) has been strongly recommended and encouraged for screening for COVID-19.[5,6] Ai et al suggested that chest CT has ultra-high sensitivity (97%) for diagnosing COVID-19.[3] Besides, excellent performance of chest CT has been reported for diagnosing cases with negative RT-PCR results.[7] Previous studies have reported the clinical and CT imaging features of COVID-19.[8,9] Typical CT findings include ground glass opacities (GGO), GGO with consolidation, crazy paving pattern, or consolidation in a peripheral, posterior, and diffuse or lower lung zone.[10–12] CT is helpful to guide clinical management and surveil the progression of COVID-19. Because of the rapid progression of COVID-19, the interval between the initial confirmation and the transfer to an intensive care unit (ICU) can be as short as a day.[11] Patients often receive more than one chest CT during their disease episode.[3,13] Hence, there is a theoretical radiation risk to these often young patients. An image modality without ionizing radiation would be of great clinical significance for evaluating COVID-19.[14]

As an image modality without ionizing radiation, magnetic resonance imaging (MRI) may be a potential alternative to CT for pulmonary application. Being less susceptible to fast T_2^* decay as well as respiratory motions, respiratory-gated ultrashort echo time MRI (UTE-MRI) has shown utility in pulmonary applications.[15–17] Ohno et al concluded that UTE-MRI could be applied for visualizing the GGO, consolidation, and so on, in high concordance with CT.[18] We therefore hypothesized that UTE-MRI may serve as a valuable technique for noninvasively assessing COVID-19. Based on the aforementioned points, this study aimed to evaluate the clinical potential of UTE-MRI for assessing COVID-19 with CT as the reference according to both a lesion-based and patient-based comparative analysis.

Materials and Methods

Patients

This prospective study was approved by the Ethical Committee of Shanghai Public Health Clinical Center. Written informed consent of each patient was obtained. From February 2020 to April 2020, a total of 36 patients were enrolled in this prospective study. The inclusion and exclusion criteria were as the follows:

Inclusion criteria:

1. Patients confirmed as COVID-19 according to the results of RT-PCR.

Exclusion Criteria:

1. The absence of UTE-MRI examinations.
2. The time interval between CT and MRI examinations was greater than 2 days.

The average time interval between the hospital admission and CT examination as well as hospital admission and MRI examination was 2.74 days (median: 3 days) and 2.87 days (median: 3 days), respectively. Ten patients were excluded because the intervals between the CT examination and UTE-MRI examination were larger than 2 days. Three patients were excluded because of the absence of UTE-MRI examination. Ultimately, this prospective study included 23 patients.

Image Acquisition

CT acquisition: CT examinations were performed with a 64-section scanner (Scenaria 64 CT; Hitachi Medical, Kashiwa, Chiba Prefecture, Japan). The scanning parameters were listed as: tube voltage, 120 kV; tube current 150–400 mA; pitch: 1.5; slice thickness: 1.0 mm; reconstructive thickness: 1 mm; collection diameter: 350 mm; reconstruction diameter: 350 mm; rotation time: 350 msec; and matrix: 512 × 512.

MRI acquisition: all MRI examinations were performed with a 3T scanner (uMR 780, United Imaging Healthcare, Shanghai, China) with a 12-channel body array combined with a 32-channel spine array. The MRI protocols included a traverse T_2-weighted fast spin echo sequence (FSE) (relaxation time [TR]: 3965 msec, echo time [TE]: 90 msec, slice thickness: 5.0 mm, field of view (FOV): 380 × 380 mm², matrix: 456 × 456), coronal T_2-weighted single-shot fast spin echo sequence (SS-FSE) (TR: 1000 msec, TE: 85 msec, slice thickness: 5.0 mm, FOV: 380 × 380 mm², matrix:

| TABLE 1. Clinical Characteristics	
Patient demographics	**No. (%)**
Median age (range)	32 (17–62)
Men	12(52.2%)
Women	11 (47.8%)
Symptoms	
Cough	11 (47.8%)
Fever	12 (52.2%)
Headache	2 (8.6%)
Sore throat	3 (13.0%)
Diarrhea	2 (8.6%)
Leukocytes	
Abnormal	3 (13.0%)
Lymphocyte	
Abnormal	6 (26.1%)
Neutrophils	
Abnormal	5 (21.7%)
Real-time PCR	
Positive	23 (100%)
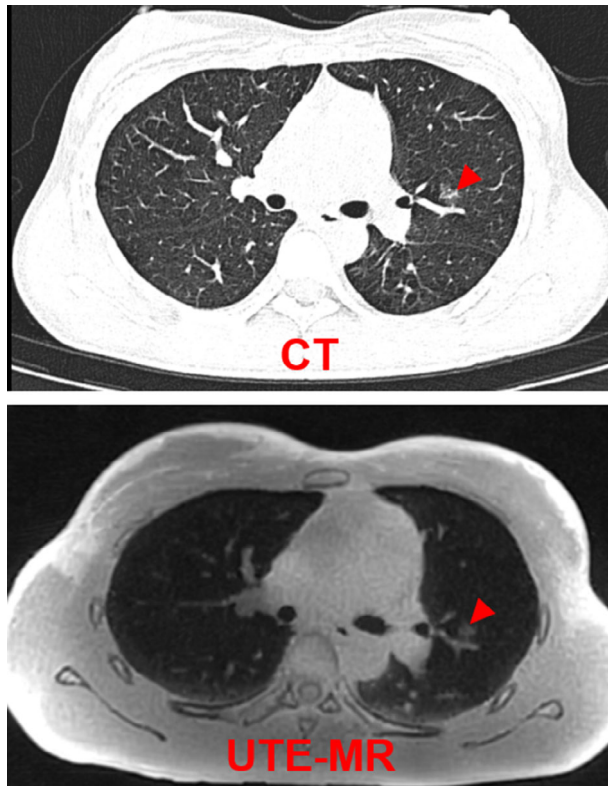
FIGURE 1: Representative CT and UTE-MRI images of a 27-year-old female patient. Radiological finding is pure GGO (red arrow).

FIGURE 2: Representative CT and UTE-MRI images of a 33-year-old female patient. Radiological findings of the pure consolidation (red arrow), GGO with consolidation (yellow arrow), air bronchogram (green arrow), and pseudocavity (blue arrow).

325×408), a respiratory-gated 3D radial UTE pulse sequence (TR: 2.2 msec, TE: 0.08 msec, flip angle [FA]: 3°, slice thickness: 2 mm, FOV: 350×350 mm^2, matrix: 480×480). Other details about the UTE-MRI protocols were: The acquisition time varied from 4–5 minutes depending on the respiration pattern of individual patients. The entire thoracic cavity was excited with a nonselective hard pulse, followed by acquisition of a free induction decay (FID) signal instead of an echo (as in the case of most conventional clinical sequences), resulting in a center-out radial encoding trajectory. Signal acquisition was initiated during the ramp-up stage of encoding gradient to further reduce the effective echo time as well as potential susceptibility artifact as a result of the air–tissue boundaries in the lung. The direction of the encoding gradient was incremented from one acquisition to another to cover the whole k-space in a "Koosh ball" pattern. A total of 40,000 encoding directions was prescribed. In order to alleviate respiratory motion artifacts, the UTE sequence was interleaved with a navigator sequence to track the diaphragm displacement in the superior–inferior direction. The acquisition module was enabled only within a certain predetermined displacement range, during which 2000 FIDs were collected each time. During reconstruction, the radial k-space data were first regridded onto Cartesian the coordinate using a Kaiser-Bessel convolution kernel.

Image Analysis

All the qualitative and quantitative assessment of CT and UTE-MRI were carried out by three experienced radiologists (S.Y.Y., with more than 6 years' experience of chest CT diagnosis and 3 years' experience of pulmonary MRI; F.S., with more than
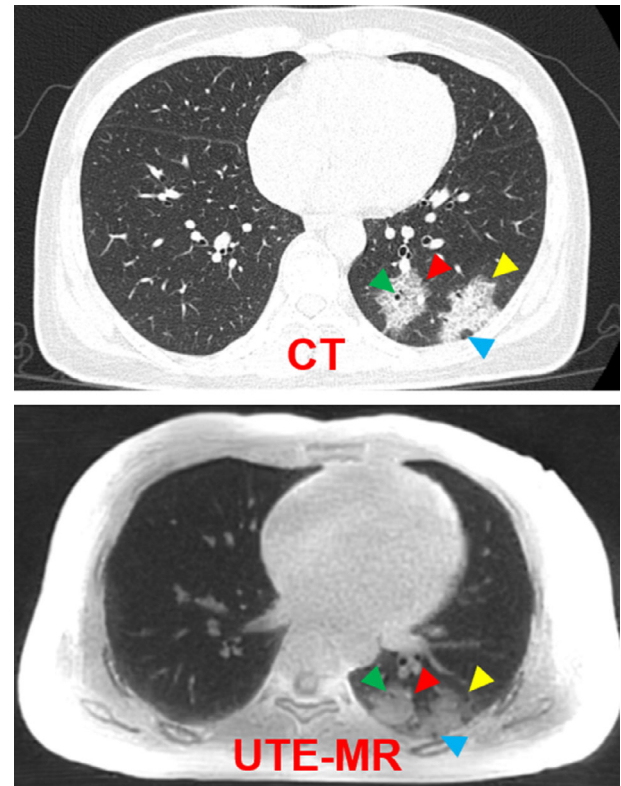
19 years' experience of chest CT diagnosis and 8 years' experience of pulmonary MRI; Z.Y.Z., with more than 36 years' experience of chest CT diagnosis and 20 years' experience of pulmonary MRI). All the CT and UTE-MRI images were randomized and independently analyzed by the above three radiologists without any information about the patients' clinical characteristics and results of other image techniques.

IMAGE QUALITY ANALYSIS. All CT and UTE-MRI images were independently scored by three radiologists with a 5-point scoring system. Detailed scoring standards were: 1: unacceptable nondiagnostic image quality, 2: poor image quality, 3: acceptable image quality, 4: good image quality, and 5: excellent image quality.

PATIENT-BASED EVALUATION. Patient-based quantitative imaging indexes including the number of affected lobes, the number of GGOs, the number of consolidations, the number of GGOs with consolidation, the number of crazy paving patterns, the number of linear opacities, total lung severity score (the sum of the severity score of each lobe; severity score of each lung lobe was based on the involvement) (score 1: none involvement [0%], score 2: minimal involvement [1–25%], score 3: mild involvement [26–50%], score 4: moderate involvement [51–75%], or score 5: severe involvement [76– 100%]) were independently evaluated by three radiologists.

LESION-BASED EVALUATION. Three radiologists independently evaluated the presence of representative image signs and
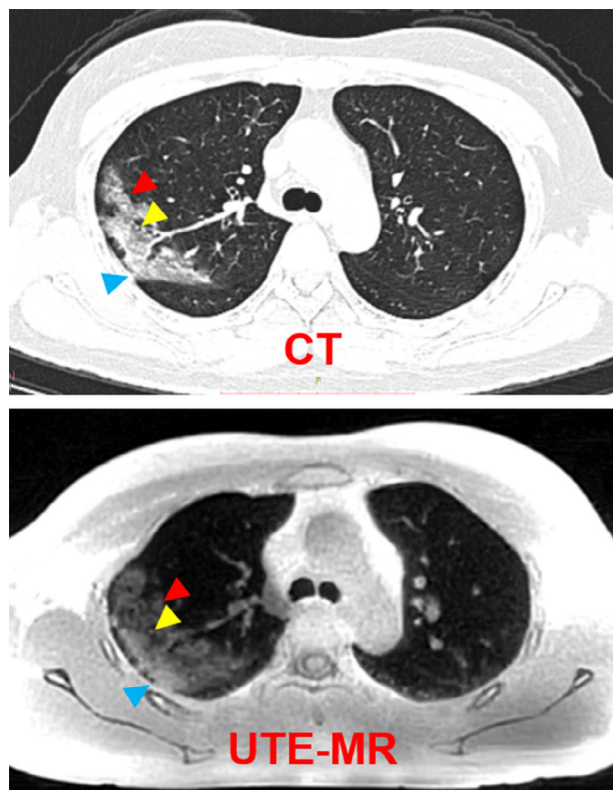
FIGURE 3: Representative CT and UTE-MRI images of a 50-year-old female patient. Radiological findings of the GGO with consolidation (red arrow) vessel expansion (yellow arrow) and pleura thickening (blue arrow).

secondary image findings of each lesion containing GGO, consolidation, GGO with consolidation, crazy-paving pattern, pseudocavity, air-bronchogram, and linear opacities via each CT and UTE-MRI images with a 5-point visual scoring system (1, absent; 2, probably absent; 3, equivocal; 4. probably present; 5, present). Also, axial location (1: central, 2: central and peripheral and 3: peripheral), anteroposterior location (1: anterior, 2: anterior and posterior and 3: posterior) were also determined by UTE-MRI and CT.

Statistical Analysis

The Shapiro–Wilk test was performed to evaluate the data normality of the image quality score. The image quality of UTE-MRI and CT was compared with a Wilcoxon-rank sum test, because both the image quality score of CT and UTE-MRI were not in normal distribution ($P < 0.05$). Kendall's coefficient of concordance (Kendall's W), intraclass coefficients (ICC), and weighted kappa statistics were calculated for determining the interobserver and intermethod agreement. The interobserver and intermethod agreement were determined as excellent for Kendall's W = 0.8–1.0, kappa = 0.8–1.0 and ICC = 0.8–1.0, substantial for Kendall's W = 0.6–0.8, kappa = 0.6–0.8 and ICC = 0.6–0.8, moderate for Kendall's W = 0.4–0.6, kappa = 0.4–0.6 and ICC = 0.4–0.6, fair for Kendall's W = 0.2–0.4, kappa = 0.2–0.4 and ICC = 0.2–0.4 as well as poor for Kendall's W = 0.0–0.2, kappa = 0.0–0.2 and ICC = 0.0–0.2. It should be noted that: 1) all the statistical results concerning the interobserver agreement evaluation were calculated by the independent evaluation of three radiologists. 2) Intermethod comparison of

image quality and patient- and lesion-based evaluation of intermethod agreement were based on the evaluation of the Z.Y.Z., who is a nationwide recognized radiologist (with more than 36 years' experience of chest CT diagnosis and 20 years' experience of pulmonary MRI). Intermethod statistical analysis was according to the previously reported method.[19] Two-sided P values of less than 0.05 were regarded as statistically significant. All the statistical analyses in this study were conducted with SPSS 26.0 (Chicago, IL).

Results

A total of 23 patients (men: 12, women: 11; median age: 32, age range: 17–62) were finally included in this study for subsequent analysis. Table 1 summarizes the clinical characteristics of the included patients.

TABLE 2. Chest Computed Tomography Findings

Radiological findings	No. (%)
No. of lobes affected	
0	0 (0%)
1	7 (30.4%)
2	5 (21.8%)
3	4 (17.4%)
4	5 (21.7%)
5	2 (8.7%)
Distribution	
Periphery distribution	22 (95.6%)
Bilateral involvement	10 (43.5%)
Multifocal involvement	20 (87.0%)
Lesion patterns	
GGO	8 (34.5%)
Consolidation	6 (26.1%)
GGO with consolidation	22 (95.7%)
Absence of both GGO and consolidation	0 (0.0%)
Air bronchogram	14 (60.9%)
Crazy paving pattern	2 (8.7%)
Linear opacities	10 (43.5%)
Other signs	
Pleural effusion	1 (4.3%)
Adjacent pleura thickening	12 (52.2%)
Vessel expansion	16 (69.6%)

TABLE 3. Interobserver Agreement for Evaluating Image Quality of CT and UTE-MRI

Methods		Image quality score					ICC	95% CI	P
		1	2	3	4	5			
CT	Reader 1	0	0	0	17	6	0.924	0.848–0.965	<0.05
	Reader 2	0	0	0	15	8			
	Reader 3	0	0	0	15	7			
UTE-MRI	Reader 1	0	0	2	18	3	0.862	0.724–0.937	<0.05
	Reader 2	0	0	2	16	5			
	Reader 3	0	0	3	17	3			
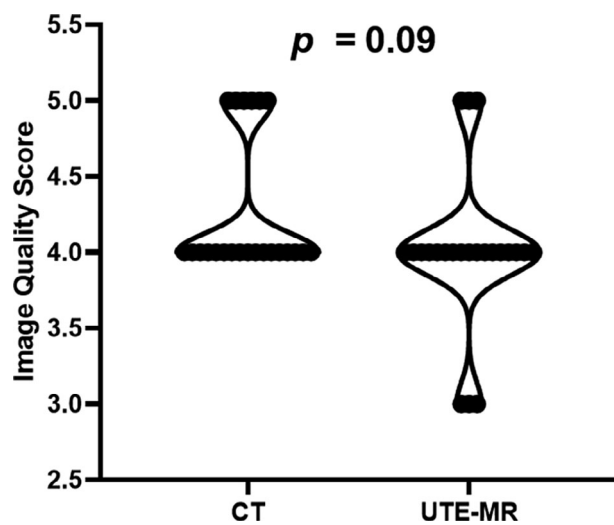
FIGURE 4: Image quality score of CT and UTE-MRI.

As shown in Table 2, chest CT examination showed that seven (30.4%) patients had one affected lobe, five (21.8%) patients had two affected lobes, four (17.4%) patients had three affected lobes, five (21.7%) patients had four affected lobes, and two (8.7%) patients had five affected lobes. In terms of lesion distribution, bilateral involvement was present in 10 (43.5%) patients and multifocal involvement was presented in 20 (87.0%) patients. GGO with consolidation was identified in 22 (95.7%) patients, pure GGO and pure consolidation were respectively identified in eight (34.5%) and six (26.1%) patients. Air bronchograms (14, 60.9%) and crazy paving patterns (two, 8.7%) were also observed within the lesion. Other secondary image findings included linear opacities (10, 43.5%), adjacent pleura thickening (12, 52.2%), vessel expansion (16, 69.6%), and pleural effusion (one, 4.3%) also occurred. Figures 1–3 demonstrate that representative radiological signs of COVID-19 including GGO, consolidation, GGO with consolidation, air bronchogram, and pseudocavity could be visualized with UTE-MRI.

Table 3 shows the interobserver ICCs of the evaluation of the image quality score of CT and UTE-MRI, which were 0.924 (P < 0.05) and 0.862 (P < 0.05). As Fig. 4 shows, there was no significant difference between the image quality of two image modalities (CT: mean score: 4.3 median score: 4.0; UTE-MRI: mean score: 4.0 median score: 4.0; Z statistics: 1.72, P = 0.09).

The results of interobserver agreement evaluation in Table 4 suggest that the interobserver ICCs of the patient-based evaluation of COVID-19 ranged between 0.939–1.000 (P < 0.05). As demonstrated in Table 5, the overall detection rate of affected lobes, GGO, consolidation, GGO with consolidation, crazy pattern, as well as linear opacities were 98.3%, 66.7%, 100%, 89.8%, 100%, and 84.6%, respectively. Moreover, intermethod ICCs of two image modalities ranged from 0.913–1.000 (P < 0.05). The total severity score quantified by CT and UTE-MRI were 2.65 and 2.65, respectively (ICC = 0.980, P < 0.05).

Kendall's W statistic was utilized for quantifying the interobserver agreement of the lesion-based evaluation of image signs, which is listed in Table 6. Table 6 demonstrates that Kendall's W was between 0.894–1.000 (P < 0.05). Lesion-based intermethod agreement of UTE-MRI and CT for assessing representative pulmonary findings of COVID-19 are shown in Table 7 and Fig. 5. A total of 100 lesions were included for the comparative analysis. The intermethod agreements for assessing the GGO, consolidation, GGO with consolidation, crazy paving pattern, pseudocavity, air bronchogram, axial location, and anteroposterior location were all statistically significant, with kappa values ranging from 0.332–1.000 (P < 0.05). Notably, the intermethod agreement for evaluating the GGO, consolidation, GGO with consolidation, axial location, and anteroposterior location was determined as substantial or excellent (kappa: 0.649–1.000, P < 0.05). As shown in Fig. 5, the visual score differences between UTE-MRI and CT for assessing the different representative signs of COVID-19 were small for most lesions. In detail, for assessing GGO, GGO with

TABLE 4. Patient-Based Interobserver Agreement for Evaluating the Representative Radiological Findings of COVID-19 With CT and UTE-MRI

Indexes	Methods	ICC	95% CI	P
No. of affected lobes	CT	1.000	1.000–1.000	<0.05
	UTE-MRI	1.000	1.000–1.000	<0.05
No. of GGO	CT	0.982	0.964–0.992	<0.05
	UTE-MRI	0.968	0.935–0.985	<0.05
No. of consolidation	CT	0.990	0.980–0.995	<0.05
	UTE-MRI	0.989	0.978–0.995	<0.05
No. of GGO with consolidation	CT	0.998	0.997–0.999	<0.05
	UTE-MRI	0.997	0.994–0.999	<0.05
No. crazy paving pattern	CT	1.000	1.000–1.000	<0.05
	UTE-MRI	0.958	0.958–0.981	<0.05
No. of linear opacities	CT	0.961	0.922–0.982	<0.05
	UTE-MRI	0.939	0.839–0.972	<0.05
Total severity score	CT	0.993	0.985–0.997	<0.05
	UTE-MRI	0.994	0.989–0.997	<0.05

TABLE 5. Patient-Based Intermethod Agreement for Evaluating the Representative Radiological Findings of COVID-19 With CT and UTE-MRI

Indexes	CT	UTE-MRI	Overall detection rate	ICC
No. of affected lobes	Mean:2.56 Total: 59.0	Mean:2.52 Total: 58.0	98.3%	0.983
No. of GGO	Mean:0.52 Total: 12.0	Mean:0.35 Total: 8.0	66.7%	0.922
No. of consolidation	Mean: 0.39 Total: 9.0	Mean: 0.39 Total: 9.0	100%	1.000
No. of GGO with consolidation	Mean: 3.82 Total: 88.0	Mean: 3.43 Total: 79.0	89.8%	0.979
No. crazy paving pattern	Mean: 0.13 Total: 3	Mean: 0.13 Total: 3	100%	1.000
No. of linear opacities	Mean: 0.56 Total: 13	Mean: 0.48 Total: 11	84.6%	0.913
Total severity score	Mean: 2.65	Mean: 2.65	—	0.980

consolidation, consolidation, pseudocavity, crazy paving pattern, and air bronchogram, the proportion of lesions with a difference in visual score less than 1 were 95.0%, 77.0%, 98.0%, 94.0%, 98.0%, and 58.0%, respectively, which indicated there was a high intermethod concordance.

TABLE 6. Lesion-Based Interobserver Agreement for Evaluating the Representative Radiological Findings of COVID-19 With CT and UTE-MRI

Radiological findings	Method	Kendall's W	*P*
GGO	CT	0.999	<0.05
	UTE-MRI	0.999	<0.05
Consolidation	CT	1.000	<0.05
	UTE-MRI	0.975	<0.05
GGO with consolidation	CT	0.941	<0.05
	UTE-MRI	0.894	<0.05
Crazy paving pattern	CT	1.000	<0.05
	UTE-MRI	0.907	<0.05
Pseudocavity	CT	0.952	<0.05
	UTE-MRI	0.949	<0.05
Air bronchogram	CT	0.963	<0.05
	UTE-MRI	0.921	<0.05
Axial location	CT	1.000	<0.05
	UTE-MRI	1.000	<0.05
Anteroposterior location	CT	1.000	<0.05
	UTE-MRI	1.000	<0.05

Kendall's W indicates the Kendall's Coefficient of Concordance.

Discussion

The results of this study suggest that there was not only high concordance between UTE-MRI and CT in assessing the representative image findings of COVID-19 but also similar image quality for two image modalities, which implies that UTE-MRI could have potential in aiding the diagnosis and surveillance of COVID-19.

The imaging findings of COVID-19 by CT have been reported recently.[7,8,20] Typical image manifestations have been described as multifocal GGO, patchy consolidation, crazy-paving pattern, air bronchogram, and multiple lesions with bilateral involvement.[21] Our study suggests that the GGO with consolidation, GGO, and bilateral and multifocal involvement with periphery distribution were the most frequently occurring CT imaging signs. Pathologically, the alveolar damage with alveolar and interstitial edema results in the appearance of GGO and crazy paving pattern.[12] As the alveoli are progressively filled with alveolar fibrinous exudate with hyaline membranes and reactive pneumocytes, GGO evolves into the appearance of consolidation.[12] Chung et al indicated that 86% of patients had the image manifestations of GGO or consolidation.[10] Similarly, Li and Xia indicated that the two principal signs of COVID-19 were GGO and consolidation.[13] However, similar to some previous studies that reported that 5–8% of confirmed COVID-19 patients were with pleural effusion[5,8,22]; pleural effusion was less frequently observed in this study.

It is known that the pulmonary application of MRI has been severely limited by respiratory motion artifact, low proton density, and fast signal decay caused by short tissue T_2^*.[23] In this study, there was no significant difference in image quality for the two methods. The results presented above indicate that UTE-MRI was capable of providing image quality similar to CT when it was utilized for evaluating COVID-19, which was concordant with several previous studies.[18,24,25] A pilot study carried out by Delacoste et al showed that UTE-MRI had image quality similar to CT for quantifying lung nodule volumes.[24] Moreover, another study revealed that submillimeter resolution could be achieved with UTE-MRI for assessing cystic fibrosis, which suggested that UTE-MRI holds promise in serving as an alternative to unenhanced CT.[25] The excellent performance of UTE-MRI for providing an image quality similar to CT was due to the following aspects. 1) Respiratory-gated MRI is effective at greatly reducing respiratory artifacts. 2) With the assistance of ultrashort echo time, UTE-MRI is capable of compromising

TABLE 7. Lesion-Based Intermethod Agreement for Evaluating the Representative Radiological Findings of COVID-19 With CT and UTE-MRI

Radiological findings	Method	Visual score					Kappa value	P
		1	2	3	4	5		
GGO	CT	92	0	0	0	8	0.815	<0.05
	UTE-MRI	91	1	3	4	1		
Consolidation	CT	94	0	0	0	6	0.876	<0.05
	UTE-MRI	92	0	0	1	7		
GGO with consolidation	CT	16	0	0	1	83	0.678	<0.05
	UTE-MRI	17	0	23	43	17		
Crazy paving pattern	CT	97	0	0	0	3	0.564	<0.05
	UTE-MRI	98	0	1	1	0		
Pseudocavity	CT	92	0	0	2	6	0.649	<0.05
	UTE-MRI	69	23	2	5	1		
Air bronchogram	CT	44	0	0	0	56	0.332	<0.05
	UTE-MRI	8	15	21	49	7		
Axial location	CT	4	0	96	—	—	1.000	<0.05
	UTE-MRI	4	0	96	—	—		
Anteroposterior location	CT	22	0	78	—	—	0.875	<0.05
	UTE-MRI	18	0	82	—	—		

the fast T_2^* signal decay, which improved the signal-to-noise ratio of images.[26]

Both the lesion- and patient-based comparative analysis showed that UTE-MRI has high concordance with CT for detecting typical pulmonary lesions, including GGO, consolidation, GGO with consolidation, axial location, anteroposterior location, the number of affected lobes, the number of crazy paving pattern, and the number of linear opacities. However, the lesion-based intermethod agreement for evaluating secondary signs such as air bronchogram, pseudocavity, and crazy paving pattern were between fair and moderate. The potential cause for this may be the lower image resolution of UTE-MRI as compared with CT. The above results are consistent with one previously reported study.[18] Ohno et al suggested that the intermethod agreement of UTE-MRI and CT for assessing the representative pulmonary findings such as GGO, consolidation, nodule, fibrosis, and so on, were all between substantial and excellent (kappa value: 0.67–0.98). UTE-MRI also displayed an image quality similar to low-dose CT. Due to the high concordance with CT for visualizing the representative pulmonary findings and an image quality similar to CT, UTE-MRI is considered valuable for evaluating the radiological findings of patients with various pulmonary parenchyma diseases.[18] Given the short supply of RT-PCR kits, which was caused by the surge in confirmed COVID-19 cases, especially in less-developed countries, and the high diagnostic sensitivity of image techniques, chest CT has been strongly encouraged for aiding prevention and control of COVID-19.[13] However, biosafety concerns are warranted due to repeated exposure of X-rays over a short period of time in the hospital. One previous cohort study demonstrated that each patient with COVID-19 underwent an average of four CT examinations within 16 days.[11] Therefore, UTE-MRI may be a valuable technique for noninvasively evaluating COVID-19.

Limitations

First, because of the strict inclusion criteria and the single-institution study, the sample size of this study was relatively small, which may have potential risk for leading to bias. Second, the CT image acquisition and UTE-MRI image acquisition were respectively performed at end-inspiration and end-expiration. Moreover, there was a time interval between CT and MRI (no more than 2 days), which was established due to consideration of the clinical process.
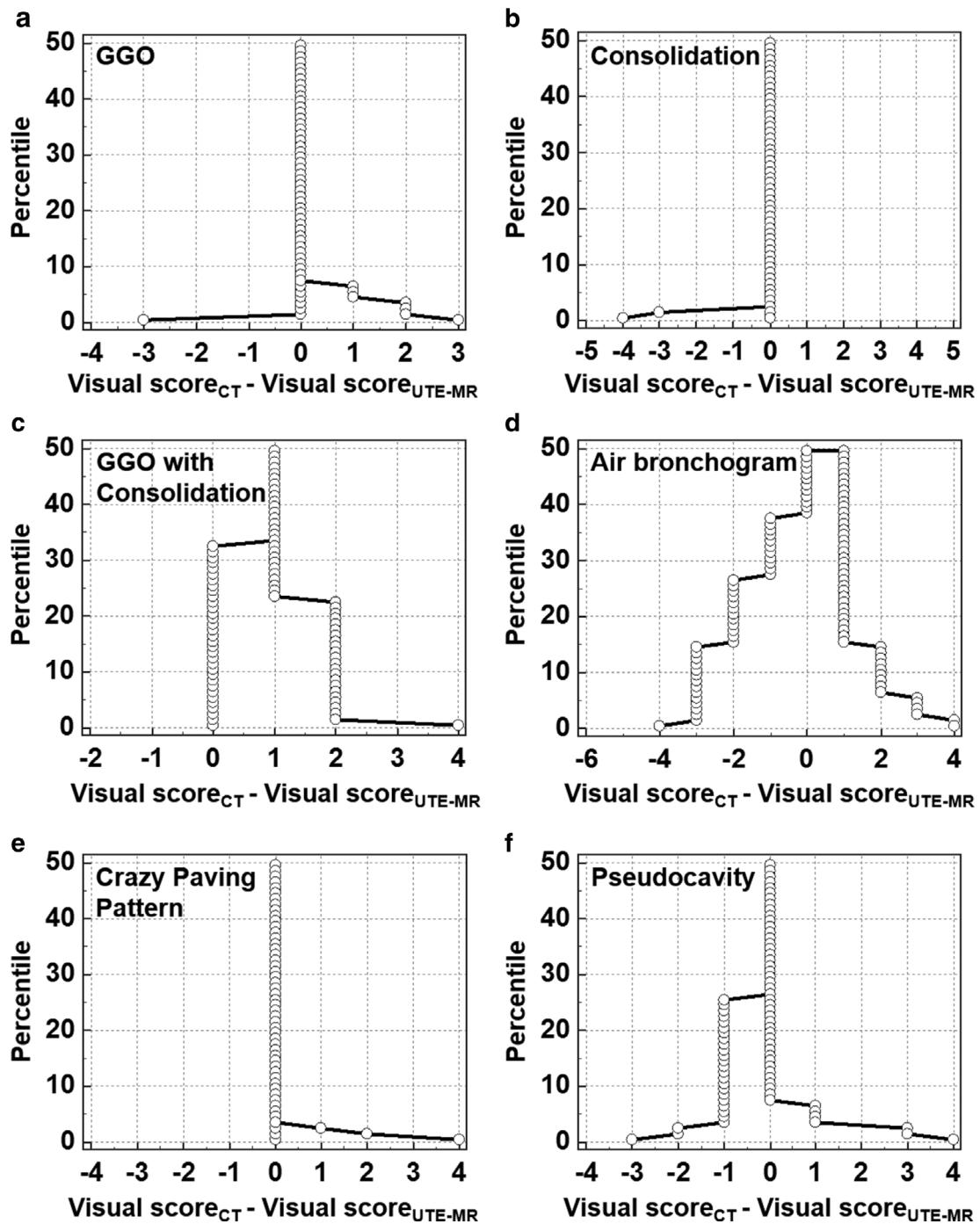
FIGURE 5: Mountain plots show the lesion-based intermethod agreement of UTE-MRI and CT for evaluating the representative image findings of COVID-19. Note: Visual score is obtained from CT and UTE-MRI for determining the presence probability of different representative image findings (1, absent; 2, probably absent; 3, equivocal; 4. probably present; 5, present).

The above issues may affect the quantification of the intermethod agreement.

suggests that UTE-MRI may act as a potential alternative to CT for noninvasively evaluating COVID-19.

Conclusion

With the continuous and rapid global spread of COVID-19, imaging examination has been widely accepted as a useful tool for aiding the control of COVID-19 patients. This study

Funding

REFERENCES

1. Coronavirus disease (COVID-2019) situation report — 104. https://www.who.int/docs/default-source/coronaviruse/situation-reports/20200503-covid-19-sitrep-104.pdf?sfvrsn=53328f46_2 (Accessed May 4, 2020).

2. Wu JT, Leung K, Leung GM. Nowcasting and forecasting the potential domestic and international spread of the 2019-nCoV outbreak originating in Wuhan, China: A modelling study. Lancet 2020;395(10225):689-697.

3. Ai T, Yang Z, Hou H, et al. Correlation of chest CT and RT-PCR testing in coronavirus disease 2019 (COVID-19) in China: A report of 1014 cases. Radiology 2020 [epub ahead of print]. https://doi.org/10.1148/radiol.2020200642.

4. Fang Y, Zhang H, Xie J, et al. Sensitivity of chest CT for COVID-19: Comparison to RT-PCR. Radiology 2020 [epub ahead of print]. https://doi.org/10.1148/radiol.2020200432.

5. Huang C, Wang Y, Li X, et al. Clinical features of patients infected with 2019 novel coronavirus in Wuhan China. Lancet 2020;395(10223):497-506.

6. Chen N, Zhou M, Dong X, et al. Epidemiological and clinical characteristics of 99 cases of 2019 novel coronavirus pneumonia in Wuhan, China: A descriptive study. Lancet 2020;395(10223):507-513.

7. Ye Z, Zhang Y, Wang Y, Huang Z, Song B. Chest CT manifestations of new coronavirus disease 2019 (COVID-19): A pictorial review. Euro Radio 2020 [epub ahead of print]. doi: https://doi.org/10.1007/s00330-020-06801-0

8. Shi H, Han X, Jiang N, et al. Radiological findings from 81 patients with COVID-19 pneumonia in Wuhan, China: A descriptive study. Lancet Infect Dis 2020;20(4):425-434.

9. Bai HX, Hsieh B, Xiong Z, et al. Performance of radiologists in differentiating COVID-19 from viral pneumonia on chest CT. Radiology 2020 [epub ahead of print]. https://doi.org/10.1148/radiol.2020200823.

10. Chung M, Bernheim A, Mei X, et al. CT imaging features of 2019 novel coronavirus (2019-nCoV). Radiology 2020;295(1):202-207.

11. Pan F, Ye T, Sun P, et al. Time course of lung changes on chest CT during recovery from 2019 novel coronavirus (COVID-19) pneumonia. Radiology 2020;295(3):715-721.

12. Xu Z, Shi L, Wang Y, et al. Pathological findings of COVID-19 associated with acute respiratory distress syndrome. Lancet Respir Med 2020;8(4):420-422.

13. Li Y, Xia L. Coronavirus disease 2019 (COVID-19): Role of chest CT in diagnosis and management. Am J Roentgenol 2020;1-7.

14. Nguyen PK, Lee WH, Li YF, et al. Assessment of the radiation effects of cardiac CT angiography using protein and genetic biomarkers. J Am Coll Cardiol Imaging 2015;8(8):873-884.

15. Bluthgen C, Wurnig MC, Jungraithmayr W, Boss A, Delacoste J. Ultrashort echo time imaging of the lungs under high-frequency noninvasive ventilation: A new approach to lung imaging. J Magn Reson Imaging 2019;50(6):1789-1797.

16. Euler A. Can texture analysis in ultrashort echo-time MRI distinguish primary graft dysfunction from acute rejection in lung transplants? A multidimensional assessment in a mouse model. Magn Reson Med 2020;51(1):108-116.

17. Pipe JG, Cleveland ZI, Woods JC, Zhu X. Iterative motion-compensation reconstruction ultra-short TE (iMoCo UTE) for high-resolution free-breathing pulmonary MRI. Magn Reson Med 2020;83(4):1208-1221.

18. Ohno Y, Koyama H, Yoshikawa T, et al. Pulmonary high-resolution ultrashort TE MR imaging: Comparison with thin-section standard- and low-dose computed tomography for the assessment of pulmonary parenchyma diseases. J Magn Reson Imaging 2016;43(2):512-532.

19. Shan F, Zhang Z, Xing W, et al. Differentiation between malignant and benign solitary pulmonary nodules: Use of volume first-pass perfusion and combined with routine computed tomography. Eur J Radiol 2012;81(11):3598-3605.

20. Wu J, Wu X, Zeng W, et al. Chest CT findings in patients with corona virus disease 2019 and its relationship with clinical features. Invest Radiol 2020;55(5):257-261.

21. Zu ZY, Jiang MD, Xu PP, et al. Coronavirus disease 2019 (COVID-19): A perspective from China. Radiology 2020 [epub ahead of print]. https://doi.org/10.1148/radiol.2020200490.

22. Yang S, Shi Y, Lu H, et al. Clinical and CT features of early-stage patients with COVID-19: A retrospective analysis of imported cases in Shanghai, China. J Euro Respir 2020 [epub ahead of print]. https://doi.org/10.1183/13993003.00407-2020

23. Chassagnon G, Martin C, Ben Hassen W, et al. High-resolution lung MRI with ultrashort-TE: 1.5 or 3 Tesla? Magn Reson Imaging 2019;61:97-103.

24. Delacoste J, Dunet V, Dournes G, et al. MR volumetry of lung nodules: A pilot study. Front Med 2019;6:18.

25. Dournes G, Menut F, Macey J, et al. Lung morphology assessment of cystic fibrosis using MRI with ultra-short echo time at submillimeter spatial resolution. Eur Radiol 2016;26(11):3811-3820.

26. Wang K, Yu H, Brittain JH, Reeder SB, Du J. K-space water-fat decomposition with T2* estimation and multifrequency fat spectrum modeling for ultrashort echo time imaging. J Magn Reson Imaging 2010;31(4):1027-1034.